Journal of Power Sources 414 (2019) 509–516

Contents lists available at ScienceDirect

Journal of Power Sources

journal homepage: www.elsevier.com/locate/jpowsour

Improving the performance of a screen-printed micro-radioisotope thermoelectric generator through stacking integration

Zicheng Yuan, Xiaobin Tang*, Yunpeng Liu, Zhiheng Xu, Kai Liu, Junqin Li, Zhengrong Zhang, Hongyu Wang

Department of Nuclear Science and Engineering, Nanjing University of Aeronautics and Astronautics, Nanjing, 211106, China

HIGHLIGHTS

- The power output of micro-RTG prototype was improved by stacking.
- Flexible circuit board was used to optimize RTG component.
- Integrated prototype powers various-color LED devices in application demo.
- Temperature effect on 10-layer prototype performance was evaluated.

GRAPHICAL ABSTRACT

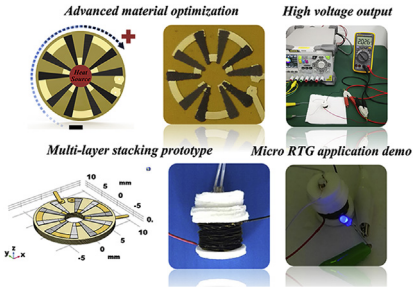

ARTICLE INFO

Keywords:
Annular–radial structure
Radioisotope thermoelectric generator
Screen printing
Series stacking

ABSTRACT

Space microscientific instruments require power supplies that are sustainable, stable, and long life. A micro-radioisotope thermoelectric generator can be used as a sustainable long-life power supply for low-power-device applications. This study innovatively proposes micro stacked-integrated annular-radial radioisotope thermoelectric generator and prepares a multilayer prototype to drive various LEDs as a demo. A high-performance micro-radioisotope thermoelectric generator module based on a flexible printed circuit is designed and prepared by screen printing. At a temperature difference of 48 K, the voltage density is 2.21 V cm^{-3}, and the power density is 514.25 μW cm^{-3}. When loaded with 1.564 W heat sources, a 10-layer prototype generates an open-circuit voltage of 0.815 V, a short-circuit current of 0.551 mA, and an output power of 114.38 μW. The maximum series voltages are 0.929 and 2.2 V for the 10- and 30-layer prototypes. The short-circuit current of the 5-layer parallel prototype is 1.18 mA, and the voltage is hardly reduced. In the impact evaluation on ambient temperature, the electrical output of the prototype increases with increased temperature (−30 °C–120 °C). In the different configurations of the prototype, the 10-layer, 30-layer series, and 5-layer parallel prototypes are proposed, thereby providing considerable output. The developed generator is expected to provide reliable power support for space microscientific instruments.

1. Introduction

A radioisotope thermoelectric generator (RTG) is a device that directly converts the decay heat of a radioisotope into electrical energy using the Seebeck effect of a thermoelectric (TE) material. The constant decay of radioisotope heat sources (e.g., ^{238}Pu and ^{90}Sr) produce heat as a system energy source. The TE module uses materials such as Bi_2Te_3, PbTe, SiGe, and skutterudite to obtain electric energy by the Seebeck

* Corresponding author.
E-mail address: tangxiaobin@nuaa.edu.cn (X. Tang).

https://doi.org/10.1016/j.jpowsour.2019.01.040
Received 3 November 2018; Received in revised form 12 January 2019; Accepted 15 January 2019
0378-7753/

Nomenclature

T	Ambient temperature (K)
α	Seebeck coefficient (μV·K^{-1})
ΔV	Voltage difference (V)
V_c	Cold-side voltage (V)
V_h	Hot-side voltage (V)
ΔT	Temperature difference (K)
T_h	Temperature of hot end (K)
T_c	Temperature of cold end (K)
V_{oc}	Open-circuit voltage (V)
I_{sc}	Short-circuit current (A)
N	Number of thermoelectric legs
α_p	P-type Seebeck coefficient (μV·K^{-1})
α_n	N-type Seebeck coefficient (μV·K^{-1})
P_{th}	Radioisotope thermal power (W)
P_{max}	Maximum output power (W)
R_{int}	Internal resistance (Ω)
R_{load}	Load resistance (Ω)
P_{load}	Load power (W)
V_{load}	Load voltage (V)
ρ_P	Power density (W cm^{-3})
ρ_V	Voltage density (V cm^{-3})
RTG	Radioisotope thermoelectric generator
TE	Thermoelectric

effect. The structure and size of the TE converter need to be optimized for different radioisotope heat sources. The power has stable output performance, sustainable operation, and strong environmental adaptability [1–6]. The miniaturized RTG can be applied in long-term service meteorological/seismic monitoring stations that are widely distributed on the surface of the planet, small landing vehicles at extreme latitudes or areas with low solar flux, atmospheric-surface-flow monitoring systems, underground detectors, deep space microspacecraft [7], wireless sensor networks [8], self-powered radiation sensors [9], deep-space robot probes [10], and radio observatories on the lunar surface [11].

The power and voltage density of a conventional RTG (MMRTG [12]) is 565 μW cm^{-3} and 0.132 mV cm^{-3}. However, this means that in a miniature version (several cubic centimeters) of RTGs, such low voltage is not directly usable. Therefore, the voltage output capability (voltage density) that can be supplied per unit volume is extremely important for micro-RTGs. Micro-RTGs consist of densely packed and small TE legs. However, developing micro-RTGs using bulk materials is challenging. Improving output performance in a limited space to increase conversion efficiency is the purpose of current studies. The advantages of this type of power supply with small size and long life are still irreplaceable by other power sources [5,13]. Thus, improving integration and performance is attracting the interest of many researchers [14,15].

Menon et al. [16,17] reported a disk device based on organic TE materials, in which 15 pairs of thermocouples are stacked in series using silver paste. Wang et al. [18] printed a large number of low-power devices consisting of bismuth telluride TE legs on a flexible printed circuit, which were in series and in parallel. The structural design of TE legs and the printing process both have a decisive impact on the prototype performance. Based on the solid heat transfer simulation model, we optimized the number and size of the TE legs to obtain the proper voltage output [19,20]. We have also improved the printing process and curing temperature to improve the electrical conductivity and Seebeck coefficient of the TE material, thereby increasing the output power of the power unit [21]. Whalen et al. [22] prepared a stacked miniaturized RTG using 11 pairs of 215 μm bulk Bi_2Te_3 materials. Gima et al. integrated 50 pairs of radial TE legs in the same plane by screen printing [23]. The above work provides some ideas for the innovation of micro-TE devices, but a trade-off remains between voltage, power, and TE legs for integrating micro-RTGs. The solution in this paper increases the number of TE legs as much as possible.

To ensure that voltage and power are suitable, we use a series and parallel mode to implement the overall structure of the micro-RTG and improve conversion efficiency. In this study, we improve the electrical performance of a micro-RTG single module. The stack connection is also investigated, and the properties of series–parallel mode and the number of layers are explored. Various micro-RTG prototypes with 10–60 layers of modules, a height of 0.225–13.5 cm, a diameter of 1.5 cm, and a volume of 1.42–5.67 cm^3 are prepared. They are tested by a loading electrically heated equivalent radioisotope heat source. Energy-conversion efficiency is improved by fabricating space-stack TE devices. The output performance of the micro-RTG at different ambient temperatures is further evaluated.

Our research team completed multilayer prototype research and manufacturing, optimized the module components, and explored the coupling mechanism and influencing factors. Given the importance of the influence of environmental factors on the micro-RTG, the temperature effect of the 10-layer prototype was studied. The output of various stacking methods is also reported, and the load capacity as a power source is discussed. Through a highly integrated process, the micro-RTG can achieve higher voltage and power per unit volume and can thus meet the voltage and power requirements of various space components. This device is expected to solve fundamental technical problems in the field of space exploration.

2. Experimental

2.1. Micro-RTG component design

As shown in Fig. 2a–c, the single-layer module of the micro-RTG consists of a polyimide substrate, connecting electrodes, and n- and p-type TE legs. After the relevant process and size-optimization design, the geometric design parameters of the component are shown in Table 1. The micro-RTG prototype comprises a series or parallel connection of multiple layers, each of which can be used as an independent functional power-generation unit. As shown in Fig. 1, the single-layer module comprises five n-type and five p-type legs. This annular–radial structure enables thermal energy to flux from the center in a radial pattern and thermal flux to flow from inside to outside through the TE legs. Gray and black elements in the figure represent p- and n-type TE semiconductors, respectively, and the temperature difference causes hole carriers and electron carriers in the semiconductor to diffuse outside (cold side) from the center (hot end). A potential gradient presents from inside to outside in p-type, which is opposite to that in n-type. After connecting the TE legs in series, the spatial potential of the single-layer module is increased counterclockwise.

The connection between layers in two multilayer stacked prototypes is shown in Fig. 2(d and e). The low potential back electrode of two

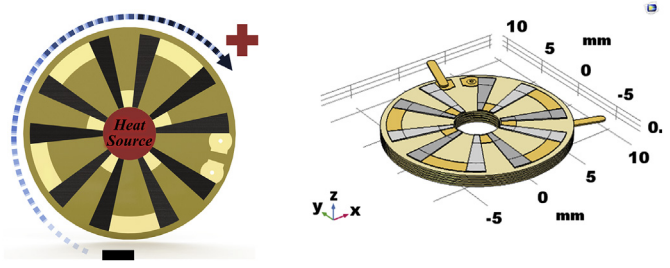

Fig. 1. Conceptual and physical simulation model.

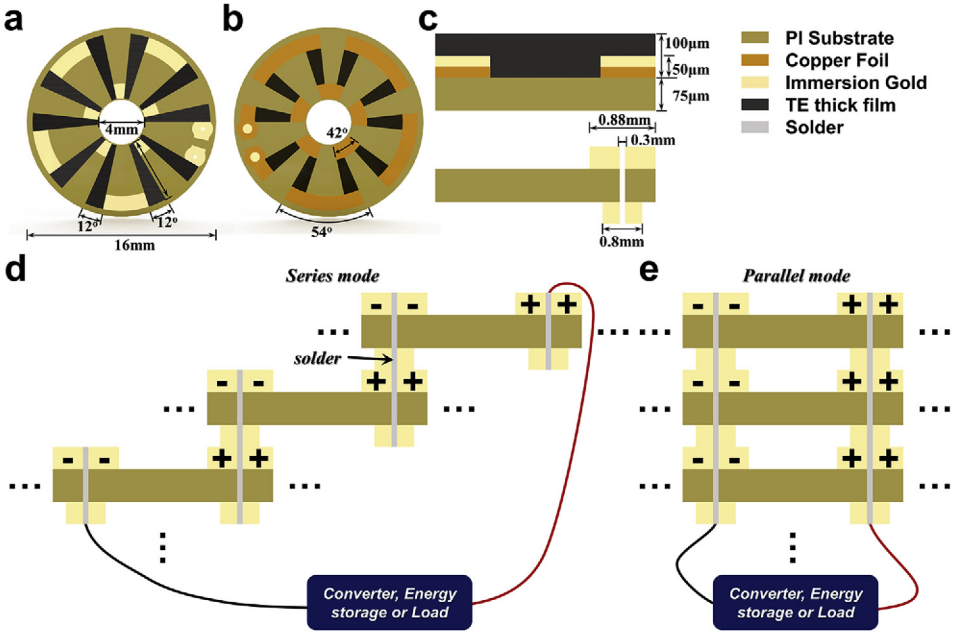

Fig. 2. Structure diagram (a) and three-dimensional view (b) of the annular radioisotope thermoelectric generator. (c) Sectional view, (d) series mode, and (e) parallel mode.

Table 1
Geometry parameters of the annular radioisotope thermoelectric generator.

Parameters	Length (mm)	Thickness (μm)	Angle (°)
PI	16 (diameter)	75	–
Copper foil	15	25	54
Immersion gold	1.25	25	54
P-type Sb_2Te_3	5.5	100	12
N-type $Bi_2Te_{2.7}Se_{0.3}$	5.5	100	12
Piercing	4	–	–

adjacent layers is welded to the front surface of the high potential electrode to form a series mode. In this mode, the thermoelectromotive force generated by each layer of components accumulates, which is a linear DC power supply in series. The internal resistance of the power source in this mode is kΩ-level, which consists of series resistance and interlayer contact resistance. According to Eqs. (5) and (6), reducing the device resistance is exceptionally critical for this design. The low–low (high–high) potential electrode welding of two adjacent layers forms a parallel mode. In this mode, the current of each layer component accumulates.

2.2. Device integration

A gold-plated copper foil circuit is initially fabricated on a polyimide-based flexible circuit board (FPC) to provide a high-performance conductive substrate for screen printing, brush coating, and electrochemical deposition (Fig. S1). Screen-printed TE legs then form a plurality of discrete RTG components. Finally, RTG components are welded in series. Immersion gold through-hole pads extend through the top and bottom surfaces as a soldered channel. In a multilayer stack connection, this approach reduces series resistance and increases current.

The following procedure is used to prepare samples with or without FPC. First, the shape of TE legs is printed onto a fixed transparent substrate to print visual alignment. TE legs used for device fabrication need to be cured twice. The polyimide film substrate used for visual alignment before printing TE legs is then fixed on a plate with preprinted patterns, and the p-type TE legs are cured at 90 °C for 30 min. Next, n-type TE legs are printed and cured at 90 °C for 30 min (Fig. 3), after which the samples used for device fabrication are cut into round slices through which a hole is punched at the center. Finally, TE legs are cured at 275 °C for 3 h.

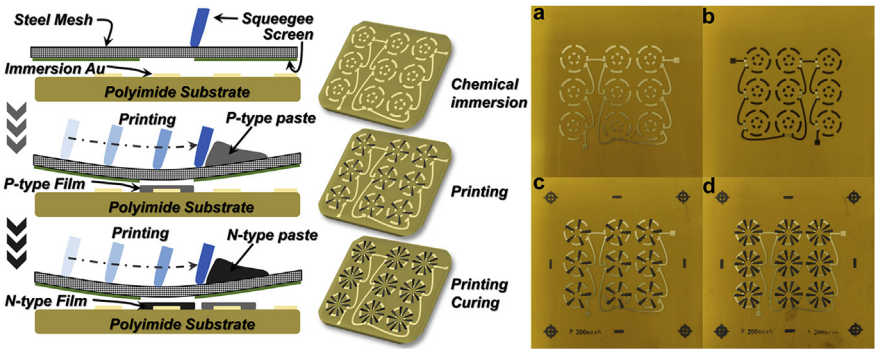

Fig. 3. FPC printing process details: (a) empty FPC, (b) back of FPC, (c) printed p-type only, and (d) print over.

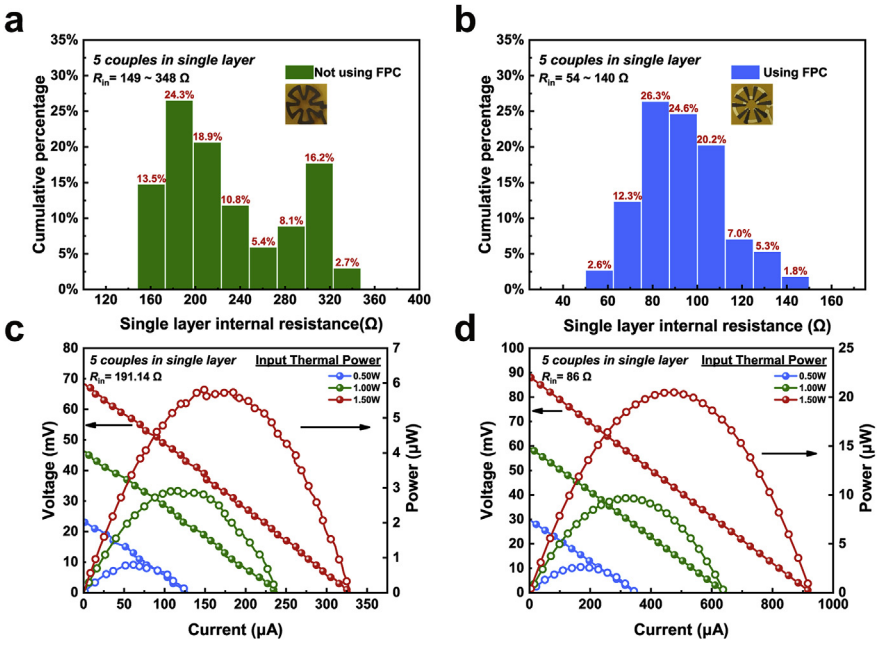

Fig. 4. (a) Without FPC, (b) with FPC, (c) output of the device without FPC, (d) and output of the device with FPC.

Table 2
Single-layer module thermoelectric-conversion electrical performance parameters after circuit optimization.

	P_{th}	I_{sc}	V_{oc}	P_{max}	ΔT
Not using FPC	0.5 W	0.128 mA	23.206 mV	0.803 μW	13.7 K
	1 W	0.239 mA	46.406 mV	2.925 μW	32.2 K
	1.5 W	0.329 mA	68.405 mV	5.811 μW	46.1 K
Using FPC	0.5 W	0.350 mA	30.005 mV	2.613 μW	16.9 K
	1 W	0.643 mA	59.504 mV	9.661 μW	32.7 K
	1.5 W	0.927 mA	88.001 mV	20.480 μW	48.3 K

Table 3
Output performance comparison of micro-RTG prototype.

P_{th}	I_{sc}	V_{oc}	P_{max}
^{3}H–Ti = 0.245 W	0.085 mA	0.113 V	1.97 μW at 0.057 V
$^{241}AmO_2$ = 0.431 W	0.150 mA	0.212 V	7.03 μW at 0.106 V
$^{90}SrTiO_3$ = 1.287 W	0.453 mA	0.668 V	75.93 μW at 0.334 V
$^{238}PuO_2$ = 1.564 W	0.551 mA	0.815 V	114.38 μW at 0.408 V

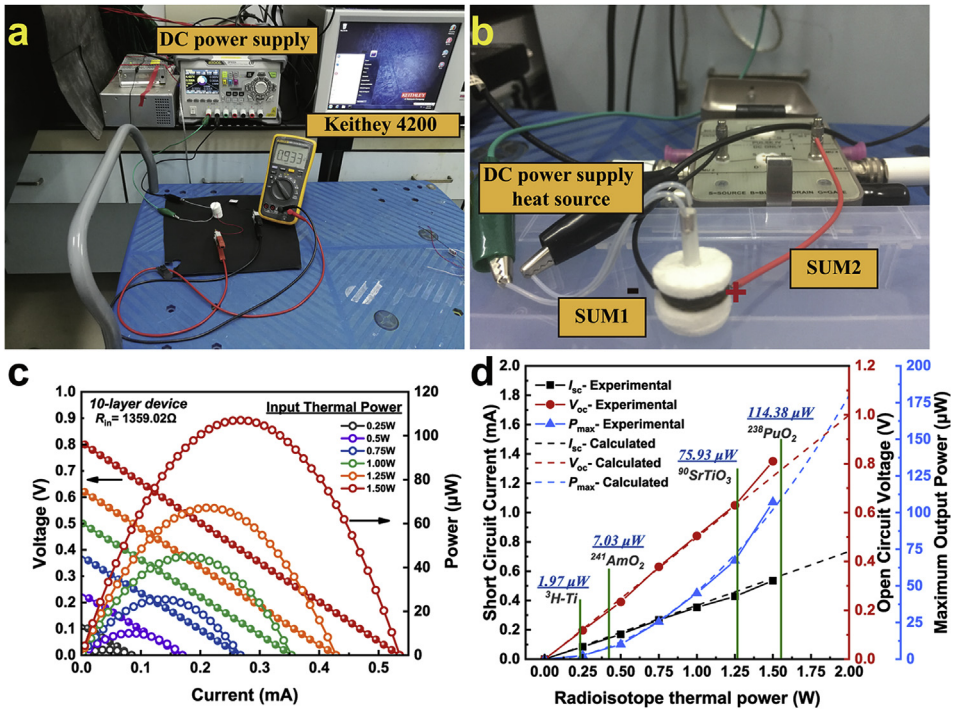

Fig. 5. Electrical performance of the 10-layer RTG. (a) Test environment and instrument. (b) Test connector details. (c and d) Relationship between heat source and electrical output.

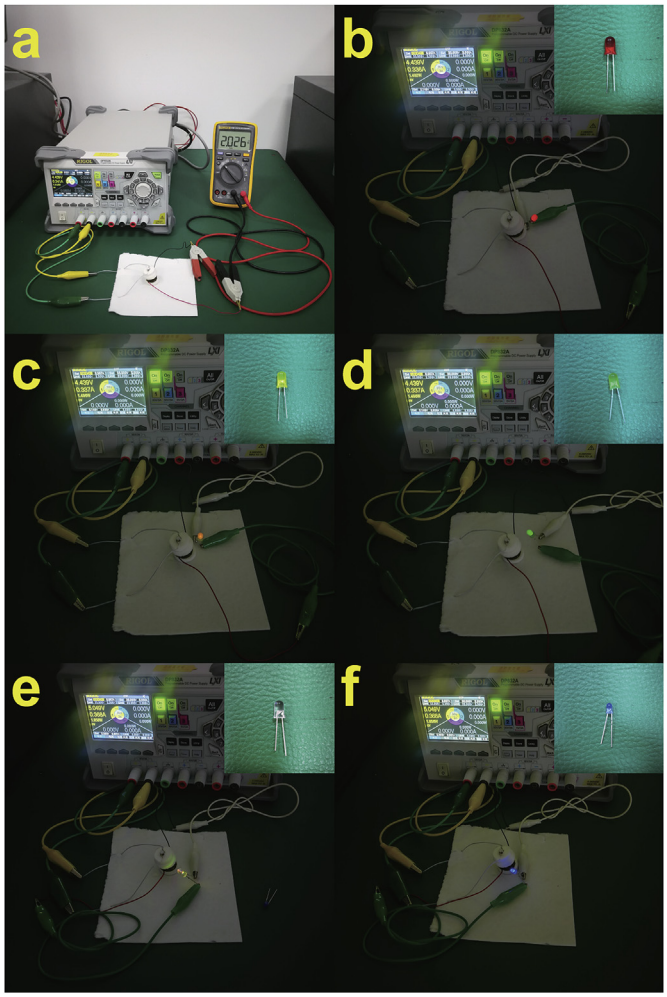

Fig. 6. A 30-layer stacked micro-RTG application in series drives the LEDs in the laboratory. (a) Multimeter measures output voltage. (b) Red LED, (c) yellow LED, (d) green LED, (e) tricolor flashing LED, and (f) blue LED. (For interpretation of the references to color in this figure legend, the reader is referred to the Web version of this article.)

2.3. Simulation calculation method

A single-layer module model is built using COMSOL Multiphysics software, meshing is performed according to the model volume microelement, and internal resistance is calculated using a constant current. Given that the voltage source is linear, the internal resistance is the slope value of the $I-V$ curve, and the equation is calculated as follows.

$$R_{\text{int}} = \frac{\Delta V}{\Delta I} \tag{1}$$

The following equation obtains the calculated value of the open-circuit voltage (V_{oc}).

$$V_{oc} = N\cdot(\alpha_{\text{p}} - \alpha_{\text{n}})\cdot\Delta T \tag{2}$$

For a 10-layer prototype, N is 50. TE material properties are measured and listed in Table S2. The value of ΔT is taken from a single-layer module.

$$\Delta V = V_{\text{c}} - V_{\text{h}} \tag{3}$$

$$\Delta T = T_{\text{h}} - T_{\text{c}} \tag{4}$$

The maximum power P_{max} is obtained by matching the external load and internal resistance of the generator, i.e., $R_{\text{load}} = R_{\text{int}}$, and it is related to V_{oc} as shown in the following equation:

$$P_{\text{max}} = \frac{{V_{\text{oc}}}^2}{4R_{\text{int}}} \tag{5}$$

The load–performance curve is plotted based on the measured values and the following equation.

$$P_{\text{load}} = \frac{{V_{\text{load}}}^2}{R_{\text{int}} + R_{\text{load}}} \tag{6}$$

2.4. Measurement of micro-RTG parameters

The heat source rod is loaded vertically into the hole, which is at the center of the radial TE leg samples. The bottom and top of the heat source rod are covered with foamed ceramic aluminum silicate fiber to reduce heat loss. A resistive joule thermal surrogate is used in the micro-RTG to simulate a radioactive fuel pellet for experimental research. The power for the heat source rods is provided by a programmable linear DC power supply (DP832A). The power range of 0–1.5 W represents the multiple heat-source columns, with the corresponding rule shown in Table S1. The experimental heat source covers the thermal power range of the above typical radioisotope heat source. J-type thermocouples are placed on the hot and cold sides of the prototype to monitor ΔT across the device. The micro-RTG is connected to a semiconductor characteristic parameter analyzer (Keithley 4200-SCS).

In the temperature-effect experiment, the variable temperature test chamber is heated in steps of 30 °C (−30 − 120 °C), and each temperature point is stable for 1 h before performing the measurements. The performance parameters of twelve 10-layer RTG prototypes with a heat source of 0–1.5 W are measured using a Keithley 2636A source meter.

3. Result and discussion

3.1. Performance of single-layer component

According to the device size and material properties, the ideal single-layer TE module has an internal resistance of 48.5 Ω. The samples are subjected to resistance sampling tests for a total of 118 samples. Measurement results show that the internal resistance of the single-layer sample produced in this experiment is mainly controlled between 70 and 110 Ω, indicating excellent electrical properties.

Fig. 4(a and b) shows the statistical results of the internal resistance experiment. Compared with the unoptimized single-layer module, resistance is significantly reduced, and the distribution is more stable and concentrated, indicating higher suitability for multilayer connection. With the FPC, performance is significantly improved.

Table 2 and Fig. 4(c and d) show the performance of single-layer components with or without FPC optimization at different heat-source powers. The maximum output power (P_{max}) reaches 20 μW, and the V_{oc} is close to one hundred millivolts. Thus, we estimate that 10 layers of similar samples can be soldered in series with a V_{oc} of several hundred millivolts and a P_{max} in the order of one hundred microwatts.

V_{oc} is found to be slightly improved. On one hand, the internal and external node circuits are not TE materials and no voltage cancellation effect is exerted; on the other hand, the thermal conductivity of the two nodes can improve ΔT.

I_{sc} increases to 281.76% because the R_{int} is reduced to 44.93%, V_{oc} increases by 28.65%, ρ_{V} 2.21 V cm^{-3}, P_{max} increases to 352.43%, and is 514.25 μW cm^{-3}.

3.2. Module electrical performance

During soldering, the internal resistance of each layer increases the contact resistance by several tens of ohms, which is an improvement compared with the kΩ-level contact resistance in some related research

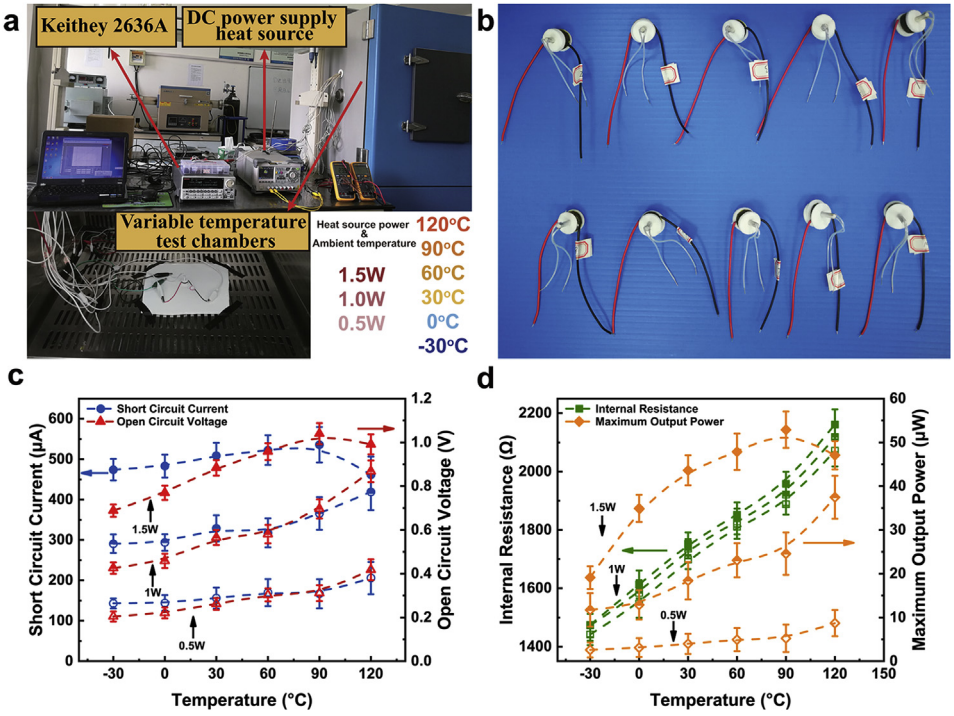

Fig. 7. Temperature dependence (−30–120 °C) of the electrical performance of 10-layer generator. (a) Temperature-change performance test equipment. (b) 10-layer RTG for testing. (c) Short-circuit current and open-circuit voltage. (d) Internal resistance and maximum output power.

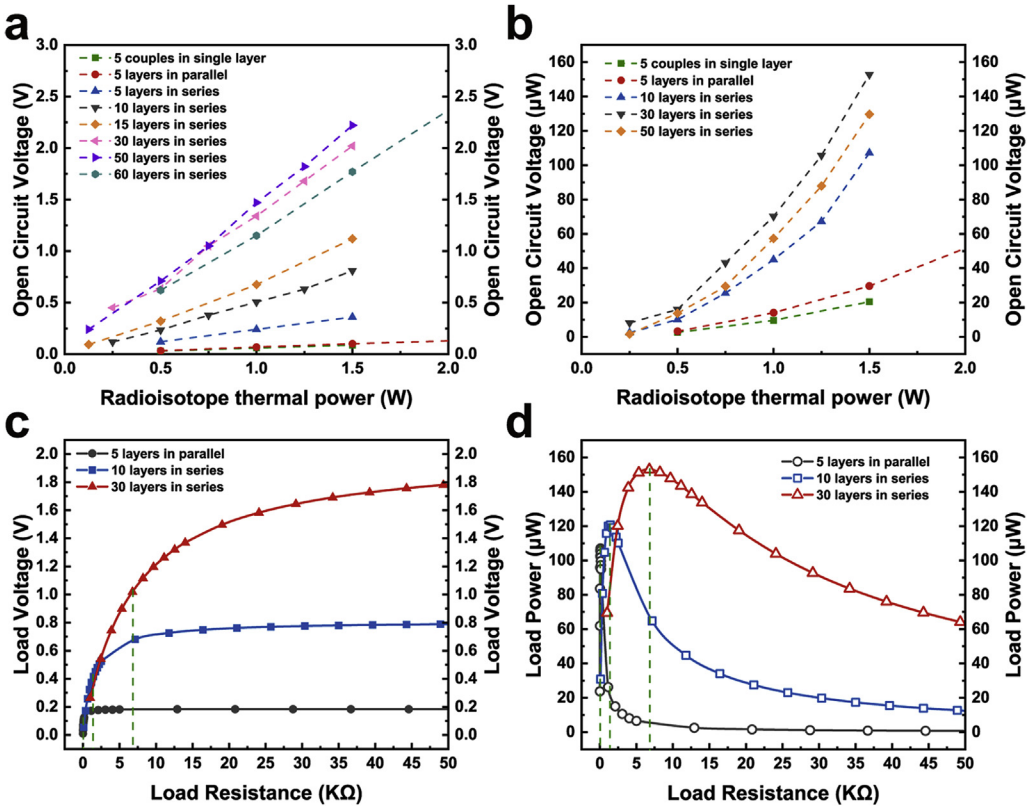

Fig. 8. (a) and (b) Micro-RTG prototype performance with different layers. (c and d) Load capability of micro-RTG power supply under a 1.5 W heat source.

work.

The open circuit voltage of the prototype is roughly observed by a multimeter (Fig. 5a). The sum1 and sum2 connect the positive and negative electrodes to the parameter analyzer for voltage sweep measurement (Fig. 5b). Current–voltage–power curves (Fig. 5c) of the micro-RTG are obtained by changing the radioisotope heat-source power of the 10-layer prototype from 0.25 W to 1.5 W. When this prototype is loaded with a heat source of 1.5 W, V_{oc} is 810.05 mV, P_{max} is 107.11 μW, and I_{sc} is 535.44 μA. With increased heating power, the output voltage and output power increase linearly and quadratically,

respectively, along with the thermal power. Internal resistance has an increasing tendency (Tables S3 and S4), and the increase is much lower than the electromotive force, so the performance impact is small. In this work, the optimization of the electrode material also curbs the above effects.

The maximum thermal power of four typical radioisotope heat-source pellets with the same volume is shown in Fig. 5d. The relationship between the electrical parameters (V_{oc}, I_{sc}, and P_{max}) of the micro-RTG and the heat-source power is shown. The detailed electrical output performance of four radioisotope heat sources is shown in Table 3. The functions of extrapolation and interpolation data are shown in Table S6.

Prototypes with different layers are also prepared for testing, the performance curve is shown in Fig. S2. The highest series voltages are as follows: 0.929 V of 10-layer, 1.12 V of 15-layer, and 2.2 V of 30-layer. The I_{sc} of the 5-layer parallel prototype is 1.18 mA, and the voltage is hardly reduced. A 30-layer micro-RTG drives various-colored LEDs, as shown in the experiment in Fig. 6 (red 1.6 V to blue 2.2 V).

3.3. Temperature effect of integrated prototype

The micro-RTG may be deployed to work in different environments in the future. To obtain the relationship between ambient temperature and performance, micro-RTG data are measured between −30 °C to 120 °C. A 10-layer series RTG device is used to evaluate performance changes due to performance and ambient temperature effects. Table S3 shows that as the heat-source power increases, the internal resistance of the module becomes higher. The internal resistance of the module increases by 12%. The performance parameters of the 10-layer prototype are related to the ambient temperature and heat source (Fig. 7). The R_{int}, V_{oc}, I_{sc}, and P_{max} of the 10-layer prototypes increase with increased temperature (−30 °C–120 °C). In the case of large heat source power, *Tc* is greater than ambient temperature due to the limitations of TE leg size. In contrast, when a low-power heat source is loaded, the Tc is close to the ambient temperature, indicating that the heat exchange is sufficient. At high ambient temperatures, the output performance of the prototype fluctuates significantly because of the temperature dependence of the TE material. This phenomenon is related to the overall heat transfer of the device possibly due to the enhancement of the mobility of the environmental convection medium. The above factors lead to increased ΔT and voltage, and the voltage increase is much more significant than the internal resistance, so the overall trend of current and power increases. However, under the condition of low heat-source power, the increase in voltage is insignificant, whereas the increase in internal resistance is constant and the increases in current and P_{max} are small.

3.4. Power-load analysis

The analysis results of output and load capacity changes for different layers are as follows (Fig. 8). V_{oc} and P_{max} in the 10–30 layer prototypes linearly accumulate. Due to the abnormal temperature-field distribution caused by heat loss, the average thermoelectromotive force of the 50–60 layer prototypes is attenuated. An uncompacted stack can generate a larger electromotive force because it is more conducive to heat dissipation than a compacted stack. With a layer count of more than 10 (in series), it can directly supply power to micro/nano-scale devices such as accelerometers and sensors. The load capacity of the power supply is analyzed, and the best application scenarios of different configurations of batteries can be understood. More series layers mean higher optimum load resistance. Specifically, the above characteristics render suitable a large number of the series modes for direct drive load. A series mode with a small number of layers is suitable for energy harvesting, storage, and reuse. Parallel mode needs to increase prototype size to enhance output voltage for energy harvesting.

4. Conclusions

We develop a microstacked-integrated annular–radial RTG for the miniaturization, stability, and long-life power supply requirements of space microscientific instruments. Manufacturing a highly integrated device is a challenge, and a new module component is designed for stacking to enhance power and voltage. The performance of the single-layer module is improved by screen printing on the FPC, resulting in a voltage density of 2.21 V cm^{-3} and a power density of 514.25 μW cm^{-3}. When loaded with a $^{238}PuO_2$ radioisotope heat source, the 10-layer prototype supplies the P_{max} of 114.38 μW at 0.408 V, short-circuit current of 0.551 mA, and open-voltage of 0.815 V. The calculation results are consistent with the experimental results. The performance parameters of different radioisotope heat sources are compared, and data reference is made for the broad practical application of micro-RTGs. Maximum series voltages measured by a multimeter are 0.929 V for 10-layer, 1.12 V for 15-layer, 2.2 V for 30-layer. A 30-layer stacked micro-RTG drives various LEDs as a demo. In different temperature environments (−30 °C–120 °C), current, voltage, and power increase with increased temperature. The load capacity of the power supply is analyzed. Different stacking schemes are found suitable for direct power supply and energy harvesting. This small, long-life power supply is ideal for distributed deep space planetary monitoring systems. This work provides new ideas and inspiration for space micropower supplies and is expected to provide long-term, stable, and reliable power supplies for space probes, deep-space wireless sensor networks, and monitoring electronics.

Acknowledgements

This work is supported by the National Natural Science Foundation of China (Grant Nos. 11675076, 11505096); the Jiangsu Planned Projects for Postdoctoral Research Funds (Grant No. 1601139B); the Funding of Jiangsu Innovation Program for Graduate Education (Grant No. KYLX16_0355); the Shanghai Aerospace Science and Technology Innovation Project (Grant No. SAST2016112).

Appendix A. Supplementary data

Supplementary data to this article can be found online at https://doi.org/10.1016/j.jpowsour.2019.01.040.

References

[1] M. Prelas, M. Boraas, F. De La Torre Aguilar, J.D. Seelig, M. Tchakoua Tchouaso, D. Wisniewski, Nuclear Batteries and Radioisotopes, (2016), https://doi.org/10.1007/978-3-319-41724-0.
[2] M.A. Prelas, C.L. Weaver, M.L. Watermann, E.D. Lukosi, R.J. Schott, D.A. Wisniewski, A review of nuclear batteries, Prog. Nucl. Energy 75 (2014) 117–148, https://doi.org/10.1016/j.pnucene.2014.04.007.
[3] B. Bairstow, Y.H. Lee, K. Oxnevad, Mission analysis for next-generation RTG study, IEEE Aerosp. Conf. Proc, 2018, https://doi.org/10.1109/AERO.2018.8396411.
[4] J.C. Bass, D.T. Allen, Milliwatt radioisotope power supply for space applications, Eighteenth Int. Conf. Thermoelectr. Proceedings, ICT'99 (Cat. No.99TH8407), 1999, https://doi.org/10.1109/ICT.1999.843443.
[5] A. Pustovalov, V. Gusev, A. Borshchevsky, A. Chmielewski, Experimental confirmation of milliwatt power source concept, Proc. ICT'99. XVIII Int. Conf. Thermoelectr, 1999.
[6] A. Khajepour, F. Rahmani, An approach to design a90Sr radioisotope thermoelectric generator using analytical and Monte Carlo methods with ANSYS, COMSOL, and MCNP, Appl. Radiat. Isot. (2017), https://doi.org/10.1016/j.apradiso.2016.11.001.
[7] B. Heshmatpour, A. Lieberman, M. Khayat, A. Leanna, T. Dobry, M.S. El-Genk, Special application thermoelectric micro isotope power sources, AIP Conf. Proc, AIP, 2008, pp. 689–695, , https://doi.org/10.1063/1.2845032.
[8] S. Roundy, D. Steingart, L. Frechette, P. Wright, J. Rabaey, Power sources for wireless sensor networks, Sens. Netw. (2004) 1–17, https://doi.org/10.1007/978-3-540-24606-0_1.
[9] N.S. Mohamed, N.G. Wright, A.B. Horsfall, Self-powered X-Ray sensors for extreme environments, Proc. IEEE Sensors, 2017, https://doi.org/10.1109/ICSENS.2017.8234008.
[10] P. Bahrami, B. Nesmith, K. Carpenter, Milli-watt radioisotope power to enable small, long-term robotic "probe" space exploration, IEEE Aerosp. Conf. Proc, 2017,

https://doi.org/10.1109/AERO.2017.7943899.
[11] R. MacDowall, Low-frequency radio observatory on the lunar surface (LROLS), Am. Astron. Soc. Meet. Abstr, vol. 232, 2018.
[12] R.G. Lange, W.P. Carroll, Review of recent advances of radioisotope power systems, Energy Convers. Manag. (2008), https://doi.org/10.1016/j.enconman.2007.10.028.
[13] V.V. Gusev, A.A. Pustovalov, N.N. Rybkin, L.I. Anatychuk, B.N. Demchuk, I.Y. Ludchak, Milliwatt-power radioisotope thermoelectric generator (RTG) based on plutonium-238, J. Electron. Mater. (2011), https://doi.org/10.1007/s11664-011-1579-z.
[14] K.V. Selvan, M.N. Hasan, M.S. Mohamed Ali, Methodological reviews and analyses on the emerging research trends and progresses of thermoelectric generators, Int. J. Energy Res. (n.d.).
[15] H. Fang, B.C. Popere, E.M. Thomas, C.K. Mai, W.B. Chang, G.C. Bazan, M.L. Chabinyc, R.A. Segalman, Large-scale integration of flexible materials into rolled and corrugated thermoelectric modules, J. Appl. Polym. Sci. (2017), https://doi.org/10.1002/app.44208.
[16] A.K. Menon, S.K. Yee, Design of a polymer thermoelectric generator using radial architecture, J. Appl. Phys. 119 (2016), https://doi.org/10.1063/1.4941101.
[17] A.K. Menon, O. Meek, A.J. Eng, S.K. Yee, Radial thermoelectric generator fabricated from n- and p-type conducting polymers, J. Appl. Polym. Sci. 134 (2017), https://doi.org/10.1002/app.44060.
[18] Z. Wang, A. Chen, R. Winslow, D. Madan, R.C. Juang, M. Nill, J.W. Evans, P.K. Wright, Integration of dispenser-printed ultra-low-voltage thermoelectric and energy storage devices, J. Micromech. Microeng. (2012), https://doi.org/10.1088/0960-1317/22/9/094001.
[19] Z. Yuan, X. Tang, Y. Liu, Z. Xu, K. Liu, Z. Zhang, W. Chen, J. Li, A stacked and miniaturized radioisotope thermoelectric generator by screen printing, Sensors Actuators, A Phys. 267 (2017) 496–504, https://doi.org/10.1016/j.sna.2017.10.055.
[20] K. Liu, X. Tang, Y. Liu, Z. Yuan, J. Li, Z. Xu, Z. Zhang, W. Chen, High-performance and integrated design of thermoelectric generator based on concentric filament architecture, J. Power Sources (2018), https://doi.org/10.1016/j.jpowsour.2018.05.018.
[21] Z. Yuan, X. Tang, Z. Xu, J. Li, W. Chen, K. Liu, Y. Liu, Z. Zhang, Screen-printed radial structure micro radioisotope thermoelectric generator, Appl. Energy (2018), https://doi.org/10.1016/j.apenergy.2018.05.073.
[22] S.A. Whalen, C.A. Apblett, T.L. Aselage, Improving power density and efficiency of miniature radioisotopic thermoelectric generators, J. Power Sources 180 (2008) 657–663, https://doi.org/10.1016/j.jpowsour.2008.01.080.
[23] Z.T. Gima, K. Gururangan, J. Evans, P. Wright, Annular screen printed thermoelectric generators for ultra-low-power sensor applications, J. Phys. Conf. Ser. (2016), https://doi.org/10.1088/1742-6596/773/1/012115.